

Dr. Arnaud Mignan
Institute of Geophysics,
Swiss Federal Institute of Technology, Zürich
NO H66, Sonneggstrasse 5
CH-8092 Zürich
arnaud.mignan@sed.ethz.ch

27 February 2018

Dear Editor Ilya Zaliapin,

Please find below my answer to your latest comment. I hope that by the few minor changes made, I correctly addressed the raised issue.

Sincerely,

Arnaud Mignan

Editor's comments

Comments to the Author:

I would like to thank the author for the next round of revisions, which further improved the readability of the paper. The revised version reveals a methodological issue that needs to be clarified.

It is stated in ll. 71-72 (marked version of the paper) that "The aim of the present article is to explain the Utsu aftershock productivity equation". At the moment it is not clear, however, how the derivations of Section 2.1 can explain the Utsu law and why the SSP is important here. Specifically, my understanding is that Eq. (12) is the final suggested explanation for the Utsu law. Furthermore, only a part of this equation — I mean $S(M)$ in some power — is used to explain the Utsu law. I list here the assumptions used to derive Eq. (12): (i) rupture surface area $S(M)$ scales with event magnitude, (ii) there exist a connected region around the mainshock rupture that accommodates the aftershocks (aftershock solid), and (iii) large EQs rupture the seismogenic layer, while small ones develop in a volume. The key equations that give the sought result are: $r(M) \sim S(M)^\alpha$ ($\alpha=1/2$ or 0 depending on the mainshock size) and $V(M) \sim r(M)S(M)$.

If my understanding is correct, the role of the SSP remains unclear. One can make multiple alternative assumptions regarding the intensity of events, and arrive at a similar scaling, which follows from straightforward geometric considerations and scaling of the surface area with magnitude. In other words, the presented derivations show that the SPP does not contradict the Utsu law, and can suggest a particular parameterization for the law's constants. This is different from "explaining" the law. Accordingly, it is important to justify the necessity of SPP in the presented derivations and separate the routine calculation of parameters (constants) from the derivation of the main scaling part of the equation.

The above issue can be readily addressed by removing the claims that SPP explains the Utsu law, and presenting SPP as a particular parameterization for this and other empirical regularities.

I modified the text accordingly, as follows:

Line 14: “We explain this law based on the SSP” changed to “We parameterize this law using the SSP”

Lines 63-69: “describe” instead of “explain”, “where the Eq. (4) scaling is parameterized using the SSP” added.

Line 342: “describe” instead of “explain”.

I however keep the term “explain” when referring to other empirical laws (foreshocks and induced seismicity) as the functional forms are directly derived from the SSP. I agree that it was not the case for aftershocks. While I provided a new formula for the aftershock production, the Utsu scaling only emerges when injecting eq. 4. This is now clarified.

Note that I also changed the specific units given in the SSP definition to “stress unit” and “number of events per unit of volume” to remain generic (lines 81-84).

1 **Utsu aftershock productivity law explained from geometric operations on the**
2 **permanent static stress field of mainshocks**

3 Arnaud Mignan*

4

5 Institute of Geophysics, Swiss Federal Institute of Technology, Zurich

6 *Address:* ETHZ, Institute of Geophysics, NO H66, Sonneggstrasse 5, CH-8092 Zurich

7

8 *Correspondence to:* arnaud.mignan@sed.ethz.ch

9

10 *Abstract:* The aftershock productivity law is an exponential function of the form
11 $K \propto \exp(\alpha M)$ with K the number of aftershocks triggered by a given mainshock of
12 magnitude M and $\alpha \approx \ln(10)$ the productivity parameter. This law remains empirical
13 in nature although it has also been retrieved in static stress simulations. Here, we
14 parameterize this law using the Solid Seismicity Postulate (SSP), the basis of a
15 geometrical theory of seismicity where seismicity patterns are described by
16 mathematical expressions obtained from geometric operations on a permanent static
17 stress field. We first test the SSP that relates seismicity density to a static stress step
18 function. We show that it yields a power exponent $q = 1.96 \pm 0.01$ for the power-law
19 spatial linear density distribution of aftershocks, once uniform noise is added to the
20 static stress field, in agreement with observations. We then recover the exponential
21 function of the productivity law with a break in scaling obtained between small and
22 large M , with $\alpha = 1.5\ln(10)$ and $\ln(10)$, respectively, in agreement with results from
23 previous static stress simulations. Possible biases of aftershock selection, verified to
24 exist in Epidemic-Type Aftershock Sequence (ETAS) simulations, may explain the
25 lack of break in scaling observed in seismicity catalogues. The existence of the
26 theoretical kink remains however to be proven. Finally, we describe how to estimate
27 the Solid Seismicity parameters (activation density δ_+ , aftershock solid envelope r_*
28 and background stress amplitude range $\Delta\sigma_*$) for large M values.

29

30 1. Introduction

31 Aftershocks, one of the most studied patterns observed in seismicity, are
32 characterized by three empirical laws, which are functions of time, such as the
33 Modified Omori law (e.g., Utsu et al., 1995), space (e.g., Richards-Dinger et al., 2010;
34 Moradpour et al., 2014), and mainshock magnitude (Utsu, 1970a; b; Ogata, 1988).

Arnaud Mignan 27.2.2018 07:40

Deleted: explain

Arnaud Mignan 27.2.2018 07:41

Deleted: based on

37 The present study focuses on the latter relationship, i.e., the Utsu aftershock
 38 productivity law, which describes the total number of aftershocks K produced by a
 39 mainshock of magnitude M as

$$40 \quad K(M) = K_0 \exp[\alpha(M - m_0)] \quad (1)$$

41 with m_0 the minimum magnitude cutoff (Utsu, 1970b; Ogata, 1988). This relationship
 42 was originally proposed by Utsu (1970a; b) by combining two other empirical laws,
 43 the Gutenberg-Richter relationship (Gutenberg and Richter, 1944) and Båth's law
 44 (Båth, 1964), respectively:

$$45 \quad \begin{cases} N(\geq m) = A \exp[-\beta(m - m_0)] \\ N(\geq M - \Delta m_B) = 1 \end{cases} \quad (2)$$

46 with N the number of events above magnitude m , A a seismic activity constant, β the
 47 magnitude size ratio (or $b = \beta/\ln(10)$ in base-10 logarithmic scale) and Δm_B the
 48 magnitude difference between the mainshock and its largest aftershock, such that

$$49 \quad K(M) = N(\geq m_0|M) = \exp(-\beta\Delta m_B) \exp[\beta(M - m_0)] \quad (3)$$

50 with $K_0 = \exp(-\beta\Delta m_B)$ and $\alpha \equiv \beta$. Eq. (3) was only implicit in Utsu (1970a) and
 51 not exploited in Utsu (1970b) where K_0 was fitted independently of the value taken by
 52 Båth's parameter Δm_B . The α -value was in turn decoupled from the β -value in later
 53 studies (e.g., Seif et al. (2017) and references therein).

54 Although it seems obvious that Eq. (1) can be explained geometrically if the
 55 volume of the aftershock zone is correlated to the mainshock surface area S with

$$56 \quad S(M) = 10^{M-4} = \exp[\ln(10)(M - 4)] \quad (4)$$

57 (Kanamori and Anderson, 1975; Yamanaka and Shimazaki, 1990; Helmstetter, 2003),
 58 there is so far no analytical, physical expression of Eq. (1) available. Although Hainzl
 59 et al. (2010) retrieved the exponential behavior in numerical simulations where
 60 aftershocks were produced by the permanent static stress field of mainshocks of

61 different magnitudes, it remains unclear how K_0 and α relate to the underlying
62 physical parameters.

63 The aim of the present article is to describe the Utsu aftershock productivity
64 equation (Eq. 1) in terms of a geometrical theory of seismicity coined “Solid
65 Seismicity”, where the Eq. (4) scaling is parameterized using the Solid Seismicity
66 Postulate (SSP). The SSP has already been shown to effectively explain other
67 empirical laws of both natural and induced seismicity from simple geometric
68 operations on a permanent static stress field (Mignan, 2012; 2016a). The theory is
69 applied here for the first time to describe aftershocks.

Arnaud Mignan 27.2.2018 07:34

Deleted: explain

Arnaud Mignan 27.2.2018 07:34

Deleted: by applying

Arnaud Mignan 27.2.2018 07:35

Deleted: (based on

Arnaud Mignan 27.2.2018 07:36

Deleted: ,

Arnaud Mignan 27.2.2018 07:36

Deleted: ,

Arnaud Mignan 27.2.2018 07:37

Deleted: which

Arnaud Mignan 27.2.2018 07:40

Deleted: the case of

71 2. Physical Expression of the Aftershock Productivity Law

72 2.1. Demonstration of the productivity law by geometric operations

73 “Solid Seismicity”, a geometrical theory of seismicity, is based on the
74 following Postulate (Mignan et al., 2007; Mignan, 2008, 2012; 2016a):

75

76 **Solid Seismicity Postulate (SSP):** *Seismicity can be strictly categorized*
77 *into three regimes of constant spatiotemporal densities δ – background*
78 *δ_0 , quiescence δ_- and activation δ_+ (with $\delta_- \ll \delta_0 \ll \delta_+$) - occurring*
79 *respective to the static stress step function:*

$$80 \delta(\sigma) = \begin{cases} \delta_- & , \sigma < -\Delta\sigma_* \\ \delta_0 & , \sigma \leq |\pm\Delta\sigma_*| \\ \delta_+ & , \sigma > \Delta\sigma_* \end{cases} \quad (5)$$

81 with σ the static stress [*stress unit*], $\Delta\sigma_*$ the background stress amplitude
82 range [*stress unit*], a stress threshold value separating two seismicity
83 regimes, and δ the spatial density of events [*number of events per unit of*
84 *volume*] per seismicity regime.

Arnaud Mignan 27.2.2018 07:47

Deleted: bar

Arnaud Mignan 27.2.2018 07:47

Deleted: bar

Arnaud Mignan 27.2.2018 07:47

Deleted: /km³

95

96 We mean by “strictly categorized” that any seismicity population is either part of the
97 background, quiescence or activation regime (or class), with no other regime/class
98 possible (i.e., a sort of hard labelling). Based on this Postulate, Mignan (2012)
99 demonstrated the power-law behavior of precursory seismicity in agreement with the
100 observed time-to-failure equation (Varnes, 1989), while Mignan (2016a)
101 demonstrated both the observed parabolic spatiotemporal front and the linear
102 relationship with injection-flow-rate of induced seismicity (Shapiro and Dinske,
103 2009). It remains unclear whether the SSP has a physical origin or not. If not, it would
104 still represent a reasonable approximation of the linear relationship between event
105 production and static stress field in a simple clock-change model (Hainzl et al., 2010;
106 Fig. 1a). For the testing of the SSP on the observed spatial distribution of aftershocks,
107 see section 2.2. The power of Eq. (5) is that it allows defining seismicity patterns in
108 terms of “solids” described by the spatial envelope $r_* = r(\sigma = \pm\Delta\sigma_*)$ where r is the
109 distance from the static stress source (e.g., mainshock rupture) and r_* the distance r at
110 which there is a change of regime (quiescence/background at $\sigma = -\Delta\sigma_*$ or
111 background/activation at $\sigma = \Delta\sigma_*$). The spatiotemporal rate of seismicity is then a
112 mathematical expression defined by the density of events δ times the volume
113 characterized by r_* (see previous demonstrations in Mignan et al. (2007) and Mignan
114 (2011; 2012; 2016a) where simple algebraic expressions were obtained).

115 In the case of aftershocks, we define the static stress field of the mainshock by

116
$$\sigma(r) = -\Delta\sigma_0 \left[\left(1 - \frac{c^3}{(r+c)^3} \right)^{-1/2} - 1 \right] \quad (6)$$

117 with $\Delta\sigma_0 < 0$ the mainshock stress drop, c the crack radius and r the distance from the
118 crack. Eq (6) is a simplified representation of stress change from slip on a planar

119 surface in a homogeneous elastic medium. It takes into account both the square root
 120 singularity at crack tip and the $1/r^3$ falloff at higher distances (Dieterich, 1994; Fig.
 121 1b). It should be noted that this radial static stress field does not represent the
 122 geometric complexity of Coulomb stress fields (Fig. 2a). However we are here only
 123 interested in the general behavior of aftershocks with Eq. (6) retaining the first-order
 124 characteristics of this field (i.e., on-fault seismicity; Fig. 2b), which corresponds to the
 125 case where the mainshock relieves most of the regional stresses and aftershocks occur
 126 on optimally oriented faults. It is also in agreement with observations, most
 127 aftershocks being located on and around the mainshock fault traces in Southern
 128 California (Fig. 2c; see section “Observations & Model Fitting”). The occasional
 129 cases where aftershocks occur off-fault (e.g., Ross et al., 2017) can be explained by
 130 the mainshock not relieving all of the regional stress (King et al., 1994; Fig. 2d).

131 For $r_* = r(\sigma = \Delta\sigma_*)$, Eq. (6) yields the aftershock solid envelope of the form:

$$132 \quad r_*(c) = \left\{ \frac{1}{\left[1 - \left(1 - \frac{\Delta\sigma_*}{\Delta\sigma_0}\right)^{-2}\right]^{1/3}} - 1 \right\} c = Fc, \quad (7)$$

133 function of the crack radius c and of the ratio between background stress amplitude
 134 range $\Delta\sigma_*$ and stress drop $\Delta\sigma_0$ (Fig. 1c). With $\Delta\sigma_0$ independent of earthquake size
 135 (Kanamori and Anderson, 1975; Abercrombie and Leary, 1993) and $\Delta\sigma_*$ assumed
 136 constant, r_* is directly proportional to c with proportionality constant, or stress factor,
 137 F (Eq. 7). Geometrical constraints due to the seismogenic layer width w_0 then yield

$$138 \quad c(M) = \begin{cases} \left(\frac{S(M)}{\pi}\right)^{1/2} & , S(M) \leq \pi w_0^2 \\ w_0 & , S(M) > \pi w_0^2 \end{cases} \quad (8)$$

139 with S the rupture surface area defined by Eq. (4) and c becoming an effective crack
 140 radius (Kanamori and Anderson, 1975; Fig. 1d). Note that the factor of 2 (i.e., using

141 w_0 instead of $w_0/2$) comes from the free surface effect (e.g., Kanamori and Anderson,
 142 1975; Shaw and Scholz, 2001).

143 The aftershock productivity $K(M)$ is then the activation density δ_+ times the
 144 volume $V_*(M)$ of the aftershock solid. For the case in which the mainshock relieves
 145 most of the regional stress, stresses are increased all around the rupture (King et al.,
 146 1994), which is topologically identical to stresses increasing radially from the rupture
 147 plane (Fig. 2a-b). It follows that the aftershock solid can be represented by a volume
 148 of contour $r_*(M)$ from the rupture plane geometric primitive, i.e., a disk or a
 149 rectangle, for small and large mainshocks, respectively. This is illustrated in Figure
 150 3a-b and can be generalized by

$$151 \quad V_*(M) = 2r_*(M)S(M) + \frac{\pi}{2}r_*^2(M)d \quad (9)$$

152 where d is the distance travelled around the geometric primitive by the geometric
 153 centroid of the semi-circle of radius $r_*(M)$ (i.e., Pappus's Centroid Theorem), or

$$154 \quad d = \begin{cases} 2\pi \left(c(M) + \frac{4}{3\pi}r_*(M) \right) & , c(M) + r_*(M) \leq \frac{w_0}{2} \\ 2w_0 & , c(M) + r_*(M) > \frac{w_0}{2} \end{cases} \quad (10)$$

155 For the disk, the volume (Eq. 9) corresponds to the sum of a cylinder of radius $c(M)$
 156 and height $2r_*(M)$ (first term) and of half a torus of major radius $c(M)$ and minus
 157 radius $r_*(M)$ (second term). For the rectangle, the volume is the sum of a cuboid of
 158 length $l(M)$ (i.e., rupture length), width w_0 and height $2r_*(M)$ (first term) and of a
 159 cylinder of radius $r_*(M)$ and height w_0 (second term; see red and orange volumes,
 160 respectively, in Figure 3a-c). Finally inserting Eqs. (7), (8) and (10) into (9), we
 161 obtain

$$162 \quad K(M) = \delta_+ \begin{cases} \left[\frac{2F}{\sqrt{\pi}} + F^2 \sqrt{\pi} \left(1 + \frac{4}{3\pi} F \right) \right] S^{3/2}(M) & , S(M) \leq \left(\frac{w_0 \sqrt{\pi}}{2(1+F)} \right)^2 \\ \frac{2F}{\sqrt{\pi}} S^{3/2}(M) + F^2 w_0 S(M) & \left(\frac{w_0 \sqrt{\pi}}{2(1+F)} \right)^2 < S(M) \leq \pi w_0^2 \\ 2F w_0 S(M) + \pi F^2 w_0^3 & , S(M) > \pi w_0^2 \end{cases}$$

163 (11)

164 which is represented in Figure 3d. Considering the two main regimes only (small
165 versus large mainshocks) and inserting Eq. (4) into (11), we get

$$166 \quad K(M) = \delta_+ \begin{cases} \left[\frac{2F}{\sqrt{\pi}} + F^2 \sqrt{\pi} \left(1 + \frac{4}{3\pi} F \right) \right] \exp \left[\frac{3 \ln(10)}{2} (M - 4) \right] & , \text{small } M \\ 2F w_0 \exp[\ln(10)(M - 4)] + \pi F^2 w_0^3 & , \text{large } M \end{cases} \quad (12)$$

167 which is a closed-form expression of the same form as the original Utsu productivity
168 law (Eq. 1). Note that K and δ_+ are both, implicitly, function of the selected minimum
169 aftershock magnitude threshold m_0 .

170 Here, we predict that the α -value decreases from $3 \ln(10)/2 \approx 3.45$ to $\ln(10) \approx$
171 2.30 when switching regime from small to large mainshocks (or from 1.5 to 1 in base-
172 10 logarithmic scale). It should be noted that Hainzl et al. (2010) observed the same
173 break in scaling in static stress transfer simulations, which corroborates our analytical
174 findings. Hainzl et al. (2010) simulated aftershocks using the clock-change model
175 where events were advanced in time by the static stress change produced by a
176 mainshock in a three-dimensional medium. They explained the scaling break
177 observed in simulation as a transition from 3D to 2D scaling regime when the
178 mainshock rupture dimension approached w_0 , which is compatible with the present
179 demonstration. For large M , the scaling is fundamentally the same as in Eq. (4). Since
180 that relation also explains the slope of the Gutenberg-Richter law (see physical
181 explanation given by Kanamori and Anderson, 1975), it follows that $\alpha \equiv \beta$, which is
182 also in agreement with the original formulation of Utsu (1970a; b; Eq. 3).

183

184 *2.2. Testing of the SSP on the aftershock spatial distribution*

185 The SSP predicts a step-like behavior of the aftershock spatial density for an
186 idealized smooth static stress field (Fig. 4a-b), which is in disagreement with real
187 aftershock observations. A number of studies have shown that the spatial linear
188 density distribution of aftershocks ρ is well represented by a power-law, expressed as
189 $\rho(r) \propto r^{-q}$ (13)
190 with r the distance from the mainshock and q the power-law exponent. This parameter
191 ranges over $1.3 \leq q \leq 2.5$ (Felzer and Brodsky, 2006; Lipiello et al., 2009; Marsan and
192 Lengliné, 2010; Richards-Dinger et al., 2010; Shearer, 2012; Gu et al., 2013;
193 Moradpour et al., 2014; van der Elst and Shaw, 2015). Although Felzer and Brodsky
194 (2004) suggested a dynamic stress origin for aftershocks, their results were later on
195 questioned by Richards-Dinger et al. (2010). Most of the studies cited above suggest
196 that the q -value is explained from a static stress process. As for the examples of
197 aftershocks shown to be dynamically triggered (e.g., Fan and Shearer, 2016), they are
198 too few to alter the aftershock productivity law and too remote to be consistently
199 defined as aftershocks in cluster methods.

200 In a more realistic setting, the static stress field must be heterogeneous (due to
201 the occurrence of previous events and other potential stress perturbations). We
202 therefore simulate the static stress field by adding a uniform random component
203 bounded over $\pm\Delta\sigma_*$ following Mignan (2011) (see also King and Bowman, 2003).
204 Note that any deviation above $\Delta\sigma_*$ would be flattened to $\Delta\sigma_*$ over time by temporal
205 diffusion (so-called “historical ghost static stress field” in Mignan, 2016a). Figure 4c
206 shows the resulting stress field and Figure 4d the predicted aftershock spatial density.
207 Adding uniform noise blurs the contour of the aftershock solid, switching the
208 aftershock spatial density from a step function (Fig. 4b) to a power-law (Fig. 4d). We

209 fit Eq. (13) to the simulated data using the Maximum Likelihood Estimation (MLE)
210 method with $r_{min} = r_*$ (Clauset et al., 2009) and find $q = 1.96 \pm 0.01$, in agreement with
211 the aftershock literature. This result alone is however insufficient to prove the validity
212 of the SSP.

213

214 **3. Observations & Model Fitting**

215 *3.1. Data*

216 We consider the case of Southern California and extract aftershock sequences
217 from the relocated earthquake catalog of Hauksson et al. (2012) defined over the
218 period 1981-2011, using the nearest-neighbor method (Zaliapin et al., 2008; used with
219 its standard parameters originally calibrated for Southern California, considering only
220 the first aftershock generation). Only events with magnitudes greater than $m_0 = 2.0$ are
221 considered (a conservative estimate following results of Tormann et al. (2014);
222 saturation effects immediately after the mainshock are negligible when considering
223 entire aftershock sequences; Helmstetter et al., 2005).

224

225 *3.2. Aftershock spatial density distribution*

226 Figure 5a represents the spatial linear density distribution of aftershocks $\rho(r)$
227 for the four largest strike-slip mainshocks in Southern California: 1987 $M=6.6$
228 Superstition Hills, 1992 $M=7.3$ Landers, 1999 $M=7.1$ Hector Mine, and 2010 $M=7.2$
229 El Mayor. The distance between mainshock and aftershocks is calculated as
230 $r = \sqrt{(x - x_0)^2 + (y - y_0)^2}$ with (x, y) the aftershock coordinates and (x_0, y_0) the
231 coordinates of the nearest point to the mainshock fault rupture (as depicted in Figure
232 2c). The dashed black lines shown in Figure 5a are visual guides to $q = 1.96$, showing
233 that the SSP is compatible with real aftershock observations.

234 Comparing Figure 5a to Figure 4d suggests that r_* can be roughly estimated
 235 from the spatial linear density plot, being the maximum distance r at which the
 236 plateau ends, here leading to $r_* \approx 1$ km. This parameter is constant for different large
 237 M values since both w_0 and $\Delta\sigma_0$ are constant while $\Delta\sigma_*$ is also *a priori* a constant. We
 238 can then estimate the ratio $\Delta\sigma_*/\Delta\sigma_0$ from Eq. (7). However the result is ambiguous
 239 due to uncertainties on the width w_0 . For $w_0 = \{5, 10, 15\}$ km, we get $\Delta\sigma_*/\Delta\sigma_0 = \{-$
 240 $0.54, -1.01, -1.38\}$.

241 As for the plateau value $\rho(r < r_*)$, it provides an estimate of the aftershock
 242 activation density δ_+ with

$$243 \delta_+ = \frac{\rho(M, r < r_*)}{\exp[\ln(10)(M-4)]} \quad (14)$$

244 a volumetric density, i.e. the linear density ρ normalized by the mainshock rupture
 245 area (Eq. 4). Due to the fluctuations in $\rho(r < r_*)$, δ_+ will be estimated from the
 246 productivity law instead (see section 3.3) and $\rho(r < r_*)$ then estimated from Eq. (14)
 247 (horizontal dashed colored lines), as detailed below.

248 It should be noted that we consider only the first-generation aftershocks to
 249 avoid ρ heterogeneities from secondary aftershock clusters occurring off-fault. An
 250 example of such heterogeneity/anisotropy is illustrated by the Landers-Big Bear case
 251 (Fig. 2c; dotted colored curve on Fig. 5a). Those cases are not systematic and
 252 therefore not considered in the aftershock productivity law. However they are also
 253 due to static stress changes (e.g., King et al., 1994) with the anisotropic effects
 254 explainable by Solid Seismicity through the concept of “historical ghost static stress
 255 field” (Mignan, 2016a).

256

257 *3.3. Aftershock productivity law*

258 The observed number n of aftershocks of magnitude $m \geq m_0$ produced by a
259 mainshock of magnitude M (for a total of N mainshocks) in Southern California is
260 shown in Figures 5b (for large $M \geq 6$) and 6a (for the full range $M \geq m_0$). We fit Eq.
261 (1) to the data using the MLE method with the log-likelihood function
262 $LL(\theta; X = \{n_i; i = 1, \dots, N\}) = \sum_{i=1}^N [n_i \ln[K_i(\theta)] - K_i(\theta) - \ln(n_i!)]$ (15)
263 for a Poisson process, representing the stochasticity of the count K of aftershocks
264 produced by a mainshock at any given time. Inserting Eq. (1) in Eq. (15) yields
265 $LL(\theta = \{K_0, \alpha\}; X) = \ln(K_0) \sum_{i=1}^N n_i + \alpha \sum_{i=1}^N [n_i (M_i - m_0)] - K_0 \sum_{i=1}^N \exp[\alpha (M_i -$
266 $m_0)] - \sum_{i=1}^N \ln(n_i!)$ (16)
267 (note that the last term can be set to 0 during LL maximization). For Southern
268 California, we obtain $\alpha_{MLE} = 2.32$ (1.01 in \log_{10} scale) and $K_0 = 0.025$ when
269 considering large $M \geq 6$ mainshocks only to avoid the issues of scaling break and data
270 dispersion at lower magnitudes. This result, represented by the black solid line on
271 Figure 5b, is in agreement with previous studies in the same region (e.g., Helmstetter,
272 2003; Helmstetter et al., 2005; Zaliapin and Ben-Zion, 2013; Seif et al., 2017) and
273 with $\alpha = \ln(10) \approx 2.30$ predicted for large mainshocks in Solid Seismicity (Eq. 12).
274 Moreover we find a bulk $\beta_{MLE} = 2.34$ (1.02 in \log_{10} scale) (Aki, 1965), in agreement
275 with $\alpha \equiv \beta$.

276 Let us now rewrite the Solid Seismicity aftershock productivity law (Eq. 12)
277 by only considering the large M case and injecting $r_* = Fw_0$ (by combining Eqs. 7-8).
278 We get
279 $K(M > M_{break}) = \delta_+ \{2r_* \exp[\ln(10)(M - 4)] + \pi r_*^2 w_0\}$ (17)
280 The role of w_0 is illustrated in Figure 5b for different values (dashed and dotted
281 curves) and shown to be insignificant for large M values. Therefore Eq. (17) can be
282 approximated to

283 $K(M > M_{break}) \approx 2\delta_+ r_* \exp[\ln(10)(M - 4)]$ (18)

284 By analogy with Eq. (1), we get

285 $\delta_+ = \frac{K_0 \exp[\ln(10)(4 - m_0)]}{2r_*}$ (19)

286 With $r_* \approx 1$ km estimated from $\rho(r)$ (section 3.2) and $K_0 = 0.025$, we obtain $\delta_+ = 1.23$
 287 events/km³ for $m_0 = 2$. We then get back the plateau $\rho(r < r_*)$ for different M values
 288 from Eq. (14), as shown in Figure 5a (horizontal dashed colored lines). Although
 289 based on limited data, this result suggests that the activation parameter δ_+ is constant
 290 (at least for large M) in Southern California. Note that if $\rho(r < r_*)$ was well
 291 constrained, it could have been estimated jointly with r_* from Figure 5a to predict the
 292 aftershock productivity law of Figure 5b without further fitting required (hence
 293 removing K_0 from the equation, K_0 having no physical meaning in Solid Seismicity).
 294

295 **4. Role of aftershock selection on productivity scaling-break**

296 We tested the following piecewise model to identify any break in scaling at
 297 smaller M , as predicted by Eq. (12):

298
$$K(M) = \begin{cases} K_0 \frac{\exp[\ln(10)(M_{break} - m_0)]}{\exp[\frac{3}{2}\ln(10)(M_{break} - m_0)]} \exp\left[\frac{3}{2}\ln(10)(M - m_0)\right] & , M \leq M_{break} \\ K_0 \exp[\ln(10)(M - m_0)] & , M > M_{break} \end{cases}$$

299 (20)

300 but with the best MLE result obtained for $M_{break} = m_0$, suggesting no break in scaling
 301 in the aftershock productivity data, as observed in Figure 6a. Final parameter
 302 estimates are $\alpha_{MLE} = 1.95$ (0.85 in log₁₀ scale) and $K_0 = 0.141$ for the full mainshock
 303 magnitude range $M \geq m_0$ (dotted line), subject to high scattering at low M values.

304 We now identify whether the lack of break in scaling in aftershock
 305 productivity observed in earthquake catalogues could be an artefact related to the

306 aftershock selection method. We run Epidemic-Type Aftershock Sequence (ETAS)
 307 simulations (Ogata, 1988; Ogata and Zhuang, 2006), with the seismicity rate

$$308 \begin{cases} \lambda(t, x, y) = \mu(t, x, y) + \sum_{i:t_j < t} K(M_i) f(t - t_i) g(x - x_i, y - y_i | M_i) \\ f(t) = c^{p-1} (p - 1) (t + c)^{-p} \\ g(x, y | M) = \frac{1}{\pi} (de^{\gamma(M-m_0)})^{q-1} (x^2 + y^2 + de^{\gamma(M-m_0)})^{-q} (q - 1) \end{cases} \quad (21)$$

309 Aftershock sequences are defined by power laws, both in time and space (for an
 310 alternative temporal function, see Mignan (2015; 2016b); the spatial power-law
 311 distribution is in agreement with Solid Seismicity in the case of a heterogeneous static
 312 stress field – see section 2.2). μ is the Southern California background seismicity, as
 313 defined by the nearest-neighbor method (with same t, x, y and m). We fix the ETAS
 314 parameters to $\theta = \{c = 0.011 \text{ day}, p = 1.08, d = 0.0019 \text{ km}^2, q = 1.47, \gamma = 2.01, \beta =$
 315 $2.29, K_0 = 0.08\}$, following the fitting results of Seif et al. (2017) for the Southern
 316 California relocated catalog and $m_0 = 2$ (see their Table 1). However, we define the
 317 productivity function $K(M)$ from Eq. (20) with $M_{break} = 5$. Examples of ETAS
 318 simulations are shown in Figure 6b for comparison with the observed Southern
 319 California time series. Figure 6c allows us to verify that the simulated aftershock
 320 productivity is kinked at M_{break} , as defined by Eq. (20).

321 We then select aftershocks from the ETAS simulations with the nearest-
 322 neighbor method. Figure 4d represents the estimated aftershock productivity, which
 323 has lost the break in scaling originally implemented in the simulations (with an
 324 underestimated $\alpha_{MLE} = 2.07$ as observed in the real case for $M \geq m_0$). Note that a
 325 similar result is obtained when using a windowing method (Gardner and Knopoff,
 326 1974). This demonstrates that the theoretical break in scaling predicted in the
 327 aftershock productivity law can be lost in observations due to an aftershock selection
 328 bias, all declustering techniques assuming continuity over the entire magnitude range.
 329 While such a bias is possible, it yet does not prove that the break in scaling exists. The

330 fact that a similar break in scaling was obtained in independent Coulomb stress
331 simulations (Hainzl et al., 2010) however provides high confidence in our results.

332 One other possible explanation for lack of scaling break is that our
333 demonstration assumes moment magnitudes while the Southern California catalogue
334 is in local magnitudes. Deichmann (2017) demonstrated that while $M_L \propto M_w$ at large
335 M , $M_L \propto 1.5M_w$ at smaller M values. This could in theory cancel the kink in real data.
336 However the scaling break predicted by Deichmann (2017) occurs at several
337 magnitude units below the geometric scaling break expected by Solid Seismicity,
338 invalidating this second option for mid-range magnitudes M .

339

340 5. Conclusions

341 In the present study, a closed-form expression defined from geometric and
342 static stress parameters was proposed (Eq. 12) to describe the empirical Utsu
343 aftershock productivity law (Eq. 1). This demonstration is similar to the previous ones
344 made by the author to explain precursory accelerating seismicity and induced
345 seismicity (Mignan, 2012; 2016b), In all these demonstrations, the main physical
346 parameters remain the same, i.e. the activation density δ_+ (also δ_- and δ_0), the
347 background stress amplitude range $\Delta\sigma_*$, and the solid envelope r_* which describes the
348 geometry of the “seismicity solid” (Fig. 3a-b). Further studies will be needed to
349 evaluate whether the δ_+ and $\Delta\sigma_*$ parameters are universal or region-specific and if the
350 same values apply to different types of seismicity at a same location.

351 Although the Solid Seismicity Postulate (SSP) (Eq. 5) remains to be proven, it
352 is so far a rather convenient and pragmatic assumption to determine the physical
353 parameters that play a first-order role in the behavior of seismicity. The similarity of
354 the SSP-simulated and observed values of the power-law exponent q of the aftershock

Arnaud Mignan 27.2.2018 08:02

Deleted: explain

356 spatial density distribution shows that the SSP is consistent with large aftershock
357 observations once uniform noise is added to the stress field (Figs. 4d-5a). The impact
358 of other types of noise on q has yet to be investigated. The SSP is also complementary
359 to the more common simulations of static stress loading (King and Bowman, 2003)
360 and static stress triggering (Hainzl et al., 2010).

361 Analytic geometry, providing both a visual representation and an analytical
362 expression of the problem at hand (Fig. 3), represents a new approach to try to better
363 understand the behavior of seismicity. Its current limitation in the case of aftershock
364 analysis consists in assuming that the static stress field is radial and described by Eq.
365 (6) (e.g., Dieterich, 1994), which is likely only valid for mainshocks relieving most of
366 the regional stresses and with aftershocks occurring on optimally oriented faults (King
367 et al., 1994). More complex, second-order, stress behaviors might explain part of the
368 scattering observed around Eq. (1) (Fig. 6a), such as overpressure due to trapped high-
369 pressure gas for example (Miller et al., 2004 – see also Mignan (2016a) for an
370 overpressure field due to fluid injection). Other $\sigma(r)$ formulations could be tested in
371 the future, the only constraint on generating so-called seismicity solids being the use
372 of the postulated static stress step function of Eq. (5) (i.e., the Solid Seismicity
373 Postulate, SSP).

374 Finally, the disappearance of the predicted scaling break in the aftershock
375 productivity law once declustering is applied (Fig. 6) indicates that more work is
376 required in that domain. Only a declustering technique that does not dictate a constant
377 scaling at all M will be able to identify rather a scaling break really exists or not.

378

379 *Acknowledgments:* I thank N. Wetzler and two anonymous reviewers, as well as
380 editor Ilya Zaliapin, for their valuable comments.

381

382 **References**

- 383 Abercrombie, R. and Leary, P.: Source parameters of small earthquakes recorded at
384 2.5 km depth, Cajon Pass, Southern California: Implications for earthquake
385 scaling, *Geophys. Res. Lett.*, 20, 1511-1514, 1993.
- 386 Aki, K.: Maximum Likelihood Estimate of b in the Formula $\log N = a - bM$ and its
387 Confidence Limits, *Bull. Earthq. Res. Instit.*, 43, 237-239, 1965.
- 388 Båth, M.: Lateral inhomogeneities of the upper mantle, *Tectonophysics*, 2, 483-514,
389 1965.
- 390 Clauset, A., Shalizi, C. R. and Newman, M. E. J.: Power-Law Distributions in
391 Empirical Data, *SIAM Review*, 51, 661-703, doi: 10.1137/070710111, 2009.
- 392 Deichmann, N.: Theoretical Basis for the Observed Break in M_L/M_w Scaling between
393 Small and Large Earthquakes, *Bull. Seismol. Soc. Am.*, 107, doi:
394 10.1785/0120160318, 2017.
- 395 Dieterich, J.: A constitutive law for rate of earthquake production and its application
396 to earthquake clustering, *J. Geophys. Res.*, 99, 2601-2618, 1994.
- 397 Fan, W. and Shearer, P. M.: Local near instantaneously dynamically triggered
398 aftershocks of large earthquakes, *Science*, 353, 1133-1136, 2016.
- 399 Felzer, K. R. and Brodsky, E. E.: Decay of aftershock density with distance indicates
400 triggering by dynamic stress, *Nature*, 441, 735-738, doi: 10.1038/nature04799,
401 2006.
- 402 Gardner, J. K. and Knopoff, L.: Is the sequence of earthquakes in Southern California,
403 with aftershocks removed, Poissonian?, *Bull. Seismol. Soc. Am.*, 64, 1363-1367,
404 1974.

405 Gu, C., Schumann, A. Y., Baisesi, M. and Davidsen, J.: Triggering cascades and
406 statistical properties of aftershocks, *J. Geophys. Res. Solid Earth*, 118, 4278-4295,
407 doi: 10.1002/jgrb.50306, 2013.

408 Gutenberg, B. and Richter, C. F.: Frequency of earthquakes in California, *Bull.*
409 *Seismol. Soc. Am.*, 34, 185-188, 1944.

410 Hainzl, S., Brietzke, G. B. and Zöller, G.: Quantitative earthquake forecasts resulting
411 from static stress triggering, *J. Geophys. Res.*, 115, B11311, doi:
412 10.1029/2010JB007473, 2010.

413 Hauksson, E., Yang, W. and Shearer, P. M.: Waveform Relocated Earthquake Catalog
414 for Southern California (1981 to June 2011), *Bull. Seismol. Soc. Am.*, 102, 2239-
415 2244, doi: 10.1785/0120120010, 2012.

416 Helmstetter, A.: Is Earthquake Triggering Driven by Small Earthquakes?, *Phys. Rev.*
417 *Lett.*, 91, doi: 10.1102/PhysRevLett.91.058501, 2003.

418 Helmstetter, A., Kagan, Y. Y. and Jackson, D. D. : Importance of small earthquakes
419 for stress transfers and earthquake triggering, *J. Geophys. Res.*, 110, B05S08, doi:
420 10.1029/2004JB003286, 2005.

421 Kanamori, H. and Anderson, D. L.: Theoretical basis of some empirical relations in
422 seismology, *Bull. Seismol. Soc. Am.*, 65, 1073-1095, 1975.

423 King, G. C. P., Stein, R. S. and Lin, J.: Static Stress Changes and the Triggering of
424 Earthquakes, *Bull. Seismol. Soc. Am.*, 84, 935-953, 1994.

425 King, G. C. P. and Bowman, D. D.: The evolution of regional seismicity between
426 large earthquakes, *J. Geophys. Res.*, 108, 2096, doi: 10.1029/2001JB000783, 2003.

427 Lin, J. and Stein, R. S.: Stress triggering in thrust and subduction earthquakes, and
428 stress interaction between the southern San Andreas and nearby thrust and strike-
429 slip faults, *J. Geophys. Res.*, 109, B02303, doi: 10.1029/2003JB002607, 2004.

430 Lippiello, E., de Arcangelis, J. and Godano, C.: Role of Static Stress Diffusion in the
431 Spatiotemporal Organization of Aftershocks, *Phys. Rev. Lett.*, 103, 038501, doi:
432 10.1103/PhysRevLett.103.038501, 2009.

433 Marsan, D. and Lengliné, O.: A new estimation of the decay of aftershock density
434 with distance to the mainshock, *J. Geophys. Res.*, 115, B09302, doi:
435 10.1029/2009JB007119, 2010.

436 Miller, S. A., Collettini, C., Chiaraluce, L., Cocco, M., Barchi, M. and Kaus, B. J. P.:
437 Aftershocks driven by a high-pressure CO₂ source at depth, *Nature*, 427, 724-727

438 Mignan, A., King, G. C. P. and Bowman, D.: A mathematical formulation of
439 accelerating moment release based on the stress accumulation model, *J. Geophys.*
440 *Res.*, 112, B07308, doi: 10.1029/2006JB004671, 2007.

441 Mignan, A.: Non-Critical Precursory Accelerating Seismicity Theory (NC PAST) and
442 limits of the power-law fit methodology, *Tectonophysics*, 452, 42-50, doi:
443 10.1016/j.tecto.2008.02.010, 2008.

444 Mignan, A.: Retrospective on the Accelerating Seismic Release (ASR) hypothesis:
445 Controversy and new horizons, *Tectonophysics*, 505, 1-16, doi:
446 10.1016/j.tecto.2011.03.010, 2011.

447 Mignan, A.: Seismicity precursors to large earthquakes unified in a stress
448 accumulation framework, *Geophys. Res. Lett.*, 39, L21308, doi:
449 10.1029/2012GL053946, 2012.

450 Mignan, A.: Modeling aftershocks as a stretched exponential relaxation, *Geophys.*
451 *Res. Lett.*, 42, 9726-9732, doi: 10.1002/2015GL066232, 2015.

452 Mignan, A.: Static behaviour of induced seismicity, *Nonlin. Processes Geophys.*, 23,
453 107-113, doi: 10.5194/npg-23-107-2016, 2016a.

454 Mignan, A.: Reply to “Comment on ‘Revisiting the 1894 Omori Aftershock Dataset
455 with the Stretched Exponential Function’ by A. Mignan” by S. Hainzl and A.
456 Christophersen, *Seismol. Res. Lett.*, 87, 1134-1137, doi: 10.1785/0220160110,
457 2016b.

458 Moradpour, J., Hainzl, S. and Davidsen, J.: Nontrivial decay of aftershock density
459 with distance in Souther California, *J. Geophys. Res. Solid Earth*, 119, 5518-5535,
460 doi: 10.1002/2014JB010940, 2014.

461 Ogata, Y.: Statistical Models for Earthquake Occurrences and Residual Analysis for
462 Point Processes, *J. Am. Stat. Assoc.*, 83, 9-27, 1988.

463 Ogata, Y. and Zhuang, J.: Space-time ETAS models and an improved extension,
464 *Tectonophysics*, 413, 13-23, doi: 10.1016/j.tecto.2005.10.016, 2006.

465 Richards-Dinger, K., Stein, R. S. and Toda, S.: Decay of aftershock density with
466 distance does not indicate triggering by dynamic stress, *Nature*, 467, 583-586, doi:
467 10.1038/nature09402, 2010.

468 Ross, Z. E., Hauksson, E. and Ben-Zion, Y.: Abundant off-fault seismicity and
469 orthogonal structures in the San Jacinto fault zone, *Sci. Adv.*, 3, doi:
470 10.1126/sciadv.1601946, 2017.

471 Seif, S., Mignan, A., Zechar, J. D., Werner, M. J. and Wiemer, S.: Estimating ETAS:
472 The effects of truncation, missing data, and model assumptions, *J. Geophys. Res.*
473 *Solid Earth*, 121, 449-469, doi: 10.1002/2016JB012809, 2017.

474 Shapiro, S. A. and Dinske, C.: Scaling of seismicity induced by nonlinear fluid-rock
475 interaction, *J. Geophys. Res.*, 114, B09307, doi: 10.1029/2008JB006145, 2009.

476 Shaw, B. E. and Scholz, C. H.: Slip-length scaling in large earthquakes: Observations
477 and theory and implications for earthquake physics, *Geophys. Res. Lett.*, 28, 2995-
478 2998, 2001.

479 Shearer, P. M.: Space-time clustering of seismicity in California and the distance
480 dependence of earthquake triggering, *J. Geophys. Res.*, 117, B10306, doi:
481 10.1029/2012JB009471, 2012.

482 Toda, S., Stein, R. S., Richards-Dinger, K. and Bozkurt, S.: Forecasting the evolution
483 of seismicity in southern California: Animations built on earthquake stress transfer,
484 *J. Geophys. Res.*, 110, B05S16, doi: 10.1029/2004JB003415, 2005.

485 Tormann, T., Wiemer, S. and Mignan, A.: Systematic survey of high-resolution b
486 value imaging along Californian faults: inference on asperities, *J. Geophys. Res.*
487 *Solid Earth*, 119, 2029-2054, doi: 10.1002/2013JB010867, 2014.

488 Utsu, T.: Aftershocks and Earthquake Statistics (1): Some Parameters Which
489 Characterize an Aftershock Sequence and Their Interrelations, *J. Faculty Sci.*
490 *Hokkaido Univ. Series 7 Geophysics*, 3, 129-195, 1970a.

491 Utsu, T.: Aftershocks and Earthquake Statistics (2): Further Investigation of
492 Aftershocks and Other Earthquake Sequences Based on a New Classification of
493 Earthquake Sequences, *J. Faculty Sci. Hokkaido Univ. Series 7 Geophysics*, 3,
494 197-266, 1970b.

495 Utsu, T., Ogata, Y. and Matsu'ura, R. S.: The Centenary of the Omori Formula for a
496 Decay Law of Aftershock Activity, *J. Phys. Earth*, 43, 1-33, 1995.

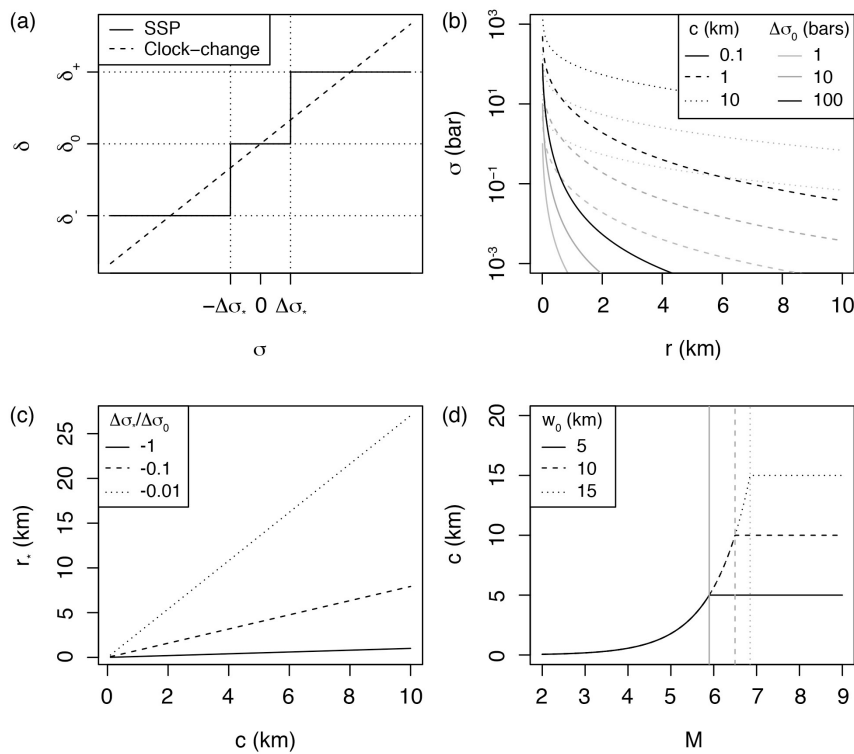
497 van der Elst, N. J. and Shaw, B. E.: Larger aftershocks happen farther away:
498 Nonseparability of magnitude and spatial distributions of aftershocks, *Geophys.*
499 *Res. Lett.*, 42, 5771-5778, doi: 10.1002/2015GL064734, 2015.

500 Varnes, D. J.: Predicting Earthquakes by Analyzing Accelerating Precursory Seismic
501 Activity, *Pure Appl. Geophys.*, 130, 661-686, 1989.

502 Yamanaka, Y. and Shimazaki, K.: Scaling Relationship between the Number of
503 Aftershocks and the Size of the Main Shock, *J. Phys. Earth*, 38, 305-324, 1990.

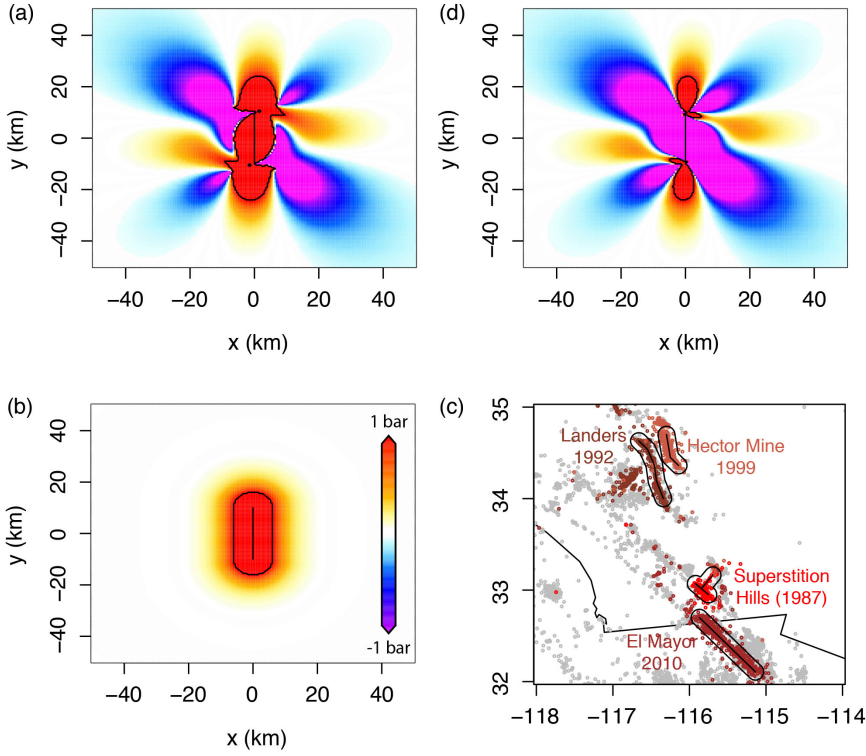
504 Zaliapin, I., Gabrielov, A., Keilis-Borok, V. and Wong, H.: Clustering Analysis of
 505 Seismicity and Aftershock Identification, Phys. Rev. Lett., 101, 018501, doi:
 506 10.1103/PhysRevLett.101.018501, 2008.
 507 Zaliapin, I. and Ben-Zion, Y.: Earthquake clusters in southern California I:
 508 Identification and stability, J. Geophys. Res. Solid Earth, 118, 2847-2864, doi:
 509 10.1002/jgrb.50179, 2013.
 510

511 **Figures**



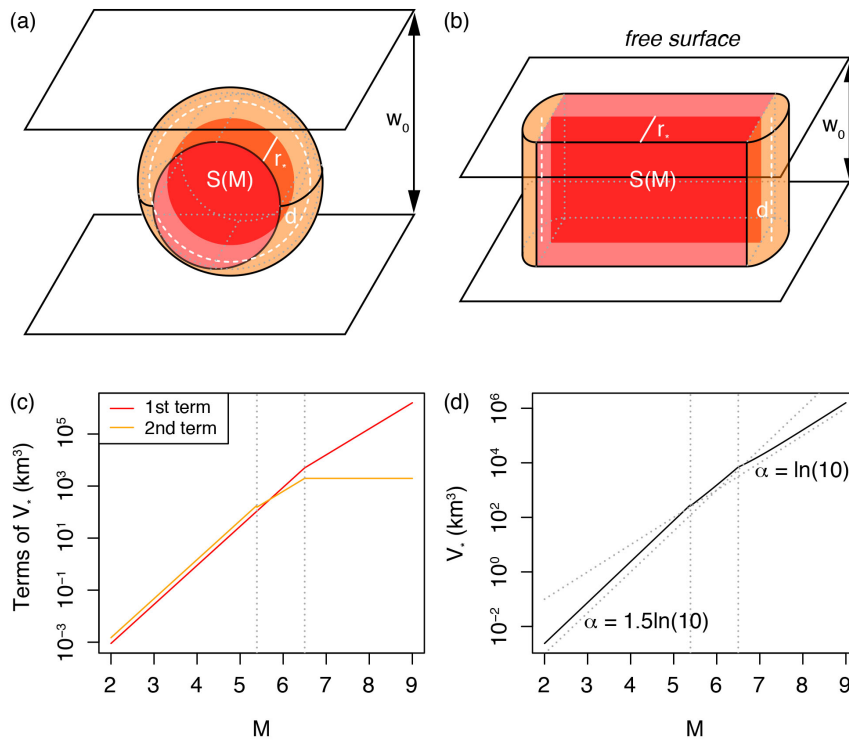
512
 513 **Figure 1.** Definition of the aftershock solid envelope in a permanent static stress field:
 514 (a) Event density stress step-function $\delta(\sigma)$ (Eq. 5) of the Solid Seismicity Postulate
 515 (SSP) in comparison to the linear clock-change model; (b) Static stress σ versus
 516 distance r for different effective crack radii c and rupture stress drops $\Delta\sigma_0$ (Eq. 6); (c)

517 Linear relationship between effective crack radius c and aftershock solid envelope
 518 radius r_* for different $\Delta\sigma_*/\Delta\sigma_0$ ratios (Eq. 7); (d) Relationship between mainshock
 519 magnitude M and effective crack radius c for different seismogenic widths w_0 (Eq. 8).
 520



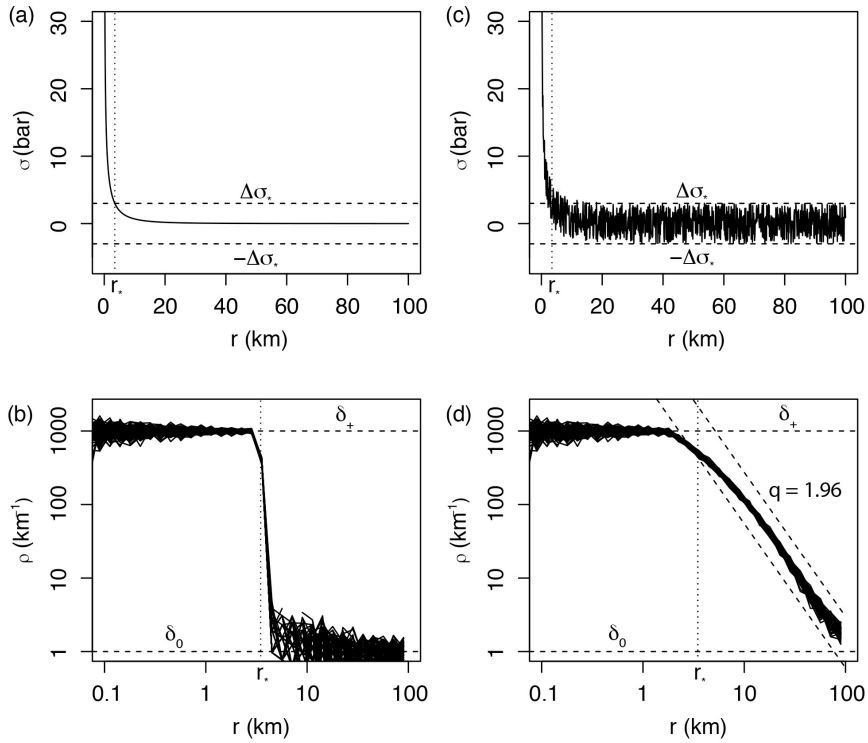
521
 522 **Figure 2.** Possible static stress fields and inferred aftershock spatial distribution: (a)
 523 Right-lateral Coulomb stress field for optimally oriented faults, where the mainshock
 524 relieves all of the regional stresses $\sigma_r = 10$ bar, with $\Delta\sigma_0 \approx -Gs/L \approx -10$ bar ($G =$
 525 $3.3 \cdot 10^5$ bar the shear modulus, $s = 0.6$ m the slip, $L = 20$ km the fault length, and $w =$
 526 10 km the fault width); (b) Radial static stress field computed from Eq. (6) with $\Delta\sigma_0 =$
 527 -10 bar and $c = \sqrt{(Lw)/\pi}$ for consistency with (a); (c) Aftershock distribution of the
 528 largest strike-slip events in the Southern California relocated catalog, identified here

529 as all events occurring within one day of the mainshock (see Data section 3.1); (d)
 530 Right-lateral Coulomb stress field for optimally oriented faults, where the mainshock
 531 relieves only a fraction of the regional stresses $\sigma_r = 100$ bar with $\Delta\sigma_0 = -10$ bar (same
 532 rupture as in (a)) – The black contour represents 1 bar in (a), (b) and (d), and a 10 km
 533 distance from rupture in (c). Coulomb stress fields of (a) and (d) were computed using
 534 the Coulomb 3 software (Lin and Stein, 2004; Toda et al., 2005).
 535



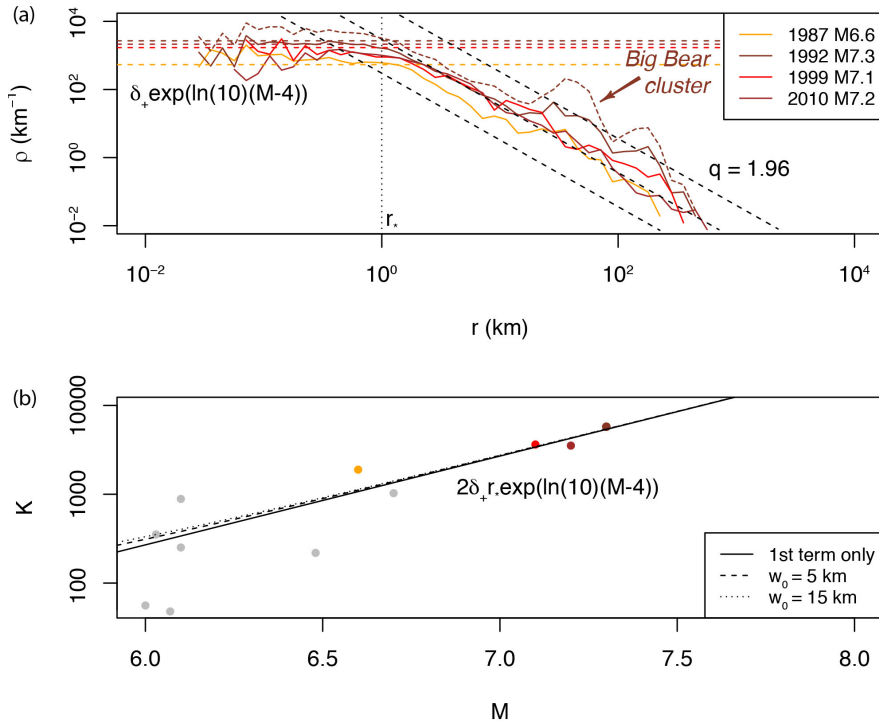
536
 537 **Figure 3.** Geometric origin of the aftershock productivity law: (a) Sketch of the
 538 aftershock solid for a small mainshock rupture represented by a disk; (b) Sketch of the
 539 aftershock solid for a large mainshock rupture represented by a rectangle; (c) Relative
 540 role of the two terms of Eq. (9), here with $w_0 = 10$ km and $\frac{\Delta\sigma_*}{\Delta\sigma_0} = -0.1$ (to first estimate
 541 c and r_* from Eqs. 8 and 7, respectively); (d) Aftershock productivity law (normalized

542 by δ_+) predicted by Solid Seismicity (Eq. 11). This relationship is of the same form as
 543 the Utsu productivity law (Eq. 1) for large M (see text for an explanation of the lack
 544 of break in scaling in Eq. 1 for small M). Dotted vertical lines represent M for
 545 $c(M) + r_*(M) = \frac{w_0}{2}$ and $S(M) = \pi w_0^2$, respectively.
 546



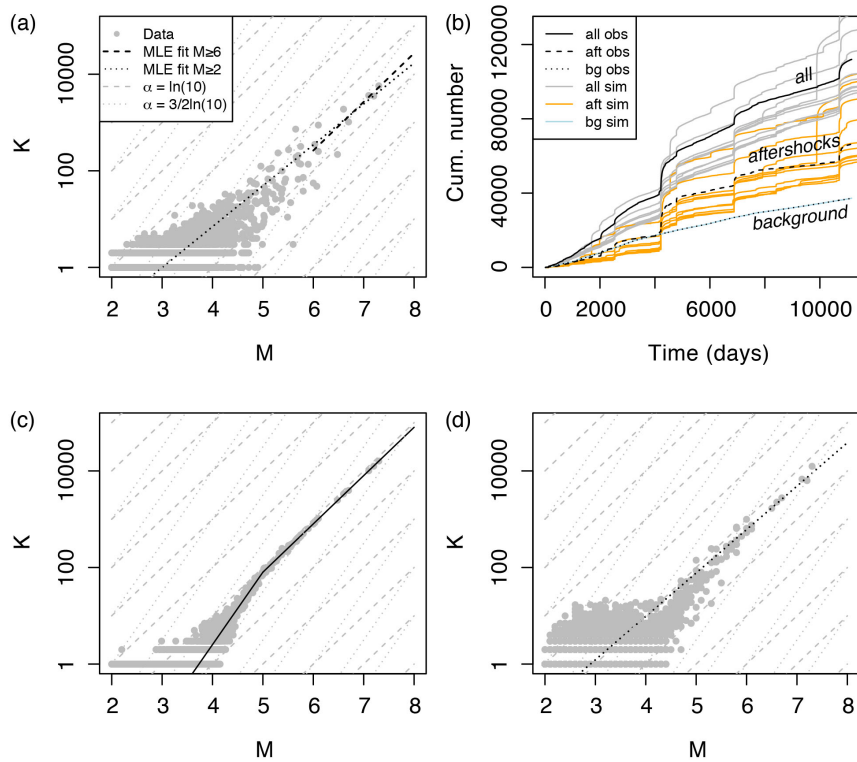
547
 548 **Figure 4.** Spatial distribution of aftershocks following the SSP. (a) Smooth static
 549 stress field as a function of distance r from the mainshock, with $\Delta\sigma_0 = -10$ bar and $c =$
 550 10 km (Eq. 6); (b) Step-like aftershock spatial linear density $\rho(r)$ with $\delta_+ = 1000$
 551 events per km, $\delta_0 = 1$ event per km and $\Delta\sigma_* = -0.3\Delta\sigma_0$ (*ad-hoc* ratio yielding $r_* = 3.5$
 552 km; Eq. (7) – event distances sampled from the $\delta(r)$ distribution, repeated 100 times).
 553 Such distribution is not observed in Nature; (c) Same as (a) but with random uniform

554 noise representative of spatial heterogeneities added to the regional stress field; (d)
 555 Power-law-like aftershock spatial linear density $\rho(r)$ with power exponent MLE
 556 estimate $q = 1.96$, representative of real aftershock observations (see Fig. 5a), due to
 557 the addition of uniform noise to the static stress field.
 558



559
 560 **Figure 5.** Estimating the Solid Seismicity parameters from the spatial distribution of
 561 aftershocks: (a) Spatial linear density distribution $\rho(r)$ of aftershocks for the four
 562 largest strike-slip mainshocks in Southern California (with first-generation
 563 aftershocks only; the density distribution comprising all aftershocks generated by the
 564 Landers mainshock is represented by the dotted curve to illustrate the type of spatial
 565 heterogeneity, such as the Big Bear cluster, not considered in the present study – see
 566 also Fig. 2c). The Solid Seismicity parameters $r_* = 1$ km and $\delta_+(m_0 = 2) = 1.23$

567 events/km³ can be retrieved from the observed plateau $\rho(r < r_*)$, in agreement with the
 568 SSP (see Fig. 4d). Note that the spatial power-law decay at high r is similar to the one
 569 expected by the SSP in the case of a static stress field with additive uniform noise
 570 (expected $q = 1.96$ represented by the dashed black lines); (b) Aftershock productivity
 571 K for $M > 6$. The curves represent the productivity law as defined by Solid Seismicity
 572 (Eq. 17) for different w_0 values (first term only corresponds to $w_0 = 0$; Eq. 18).
 573



574
 575 **Figure 6.** Aftershock productivity defined as the number of aftershocks $K(m_0 = 2)$ per
 576 mainshock of magnitude M : (a) Observed aftershock productivity in Southern
 577 California with aftershocks selected using the nearest-neighbor method; (b)
 578 Seismicity time series with distinction made between background events and

579 aftershocks, observed (“obs”, in black) and ETAS-simulated (“sim”, colored); (c)
580 True simulated aftershock productivity with kink, defined from Eq. (20); (d)
581 Retrieved simulated aftershock productivity with aftershocks selected using the
582 nearest-neighbor method - Data points in (a), (c) and (d) are represented by grey dots;
583 the model MLE fits are represented by the dashed and dotted black lines for $M \geq 6$
584 and $M \geq m_0$, respectively; dashed and dotted grey lines are visual guides to $\alpha =$
585 $3/2\ln(10)$ and $\ln(10)$, respectively.
586